EARTH'S CRYOSPHERE
SCIENTIFIC JOURNAL

Earth's Cryosphere, 2022, vol. XXVI, No. 3, pp. 43–53

SNOW COVER AND GLACIERS

MODELING OF DEBRIS FLOW TRIGGERED BY SNOW MELTING: CASE STUDY OF THE BARSEMDARA RIVER, TAJIKISTAN

V.A. Iudina (Kurovskaia)[1,*], S.S. Chernomorets[1], T.A. Vinogradova[2], I.N. Krylenko[1,3]

[1] *Lomonosov Moscow State University, Faculty of Geography, Leninskie gory 1, Moscow, 119991 Russia*
[2] *Research and Production Association Gidrotekhproekt LLC, ul. Oktyabrskaya 55A, Valdai, Novgorod oblast, 175400 Russia*
[3] *Water Problems Institute, Russian Academy of Sciences, ul. Gubkina 3, Moscow, 119333 Russia*

**Corresponding author; e-mail: viktoriiakurovskaia@gmail.com*

One of the latest catastrophic debris flow disasters took place in the Barsemdara River valley (Tajikistan) in 2015. The aim of this study was to apply chain modeling to consider the characteristics of this debris flow. This approach was also applied to assess potential flood-prone zones for future debris flows. To consider the characteristics of debris flow in the source, the transport-shift model developed by Yu.B. Vinogradov was applied. Based on this model, debris flow hydrographs were obtained and used as input data for valley zoning based on the FLO-2D model. So, for scenario I, the debris flow discharge of the forward wave (maximum 1630 m^3/s) was used as the input hydrograph; for scenario II, the debris flow discharge at the source outlet (maximum 650 m^3/s) was used. The digital elevation model ALOS PALSAR (12.5 m) was used as the relief data. As there were no rheological data, the modeling was carried out using several sets of parameters. The simulated debris flow discharges based on the most realistic option for scenario I varied from 1494 to 2860 m^3/s for individual waves. Additionally, the authors carried out modeling using digital elevation model from an unmanned aerial vehicle obtained during the survey in 2019. The results showed that the considered approach makes it possible to estimate the boundaries of both actual and potential flood-prone zones.

Keywords: *debris flow, Barsemdara River, transport-shift debris flow formation model, FLO-2D model, Pamir Mountains.*

***Recommended citation*:** Iudina (Kurovskaia) V.A., Chernomorets S.S., Vinogradova T.A., Krylenko I.N., 2022. Modeling of debris flow triggered by snow melting: case study of the Barsemdara River, Tajikistan. *Earth's Cryosphere*, XXVI (3), 43–53.

INTRODUCTION

In 1969–2015, eight catastrophic debris flow disasters were documented in the Gorno-Badakhshan Autonomous Oblast (GBAO) of Tajikistan. Information about individual rainstorm-induced debris flow events from 2007 to 2010 was presented by I. Mal'neva and N. Kononova [*2012*]. In 2002, glacial debris flow caused by lake outburst took place in the Dasht River valley. Assessment of catastrophic debris flow characteristics by modeling with FLO-2D and RAMMS was given in [*Mergili et al., 2011*]. The latest mass debris flow events in the Barsemdara River valley were observed in July 2015. Glacial origin of largest debris flows is normally considered, while the role of snowmelt as the main control is often underestimated. In the GBAO, there are 6650 glaciers in the GBAO, and their total area reaches 6785.6 km^2 [*Osipova, 1978; Shchetinnikov, Podkopaeva, 1978; Varnakova, Rototaeva, 1978, 1979; Shchetinnikov, 1979; Musoev, Atlas, 1980; Tukeev, 2002*], or 5.4% of the total glaciated area in Eurasia [*Kotlyakov, 1984*]. Despite the presence of a glacier in the Barsemdara River catchment, snowmelt was the main trigger of catastrophic debris flow events [*Dokukin et al., 2019*].

During the debris flow disaster in 2015, a debris fan dammed the Gunt River, which resulted in the appearance of a dammed lake that was later named Barsemkul' Lake. This led to the flooding of about 70 households, more than two kilometers of the highway connecting Tajikistan with China and Kyrgyzstan, five bridges (three road and two pedestrian), medical center, school, retail outlets, orchards, and fertile land, including tens of kilometers of irrigation networks. The main high-voltage power supply line from the Pamir-1 hydropower plant was also destroyed [*Chernomorets et al., 2015*].

Debris flow characteristics were determined based on visual observation and satellite data analysis [*Chernomorets et al., 2015; Keiler et al., 2018; Dokukin et al., 2019*]. Earlier, authors of this paper assessed discharges of debris flow using transport-shift model and video footage [*Kurovskaia et al., 2020*]. The aim of this work is the application of chain modelling to consider the increment of material in the source and valley zoning for the debris flow of 2015, as well as the flood zone assessment. The particular tasks included (i) preparation of digital elevation model,

(ii) improvement of the transport-shift model [*Vinogradov, 1980a,b*], (iii) selection of necessary parameters for modelling in FLO-2D software, and (iv) calculations and quality assessment.

STUDY OBJECT

The Barsemdara River is the right tributary of the Gunt River and belongs to the Panj (Pyandzh) River catchment. The river length is 8.6 km, and its catchment area is 28 km^2. Mean and maximum elevations within the catchment are 3912 and 4919 m asl, respectively. There were at least 14 series of debris flow events documented for the period of 16 to 20 of July 2015. The total amount of debris flow waves varied from 30 to 40 according to M. Keiler [*Keiler et al., 2018*]. Debris flow sites were at the elevation of ca. 4100 m in the upper part of the Barsemdara's headwaters from the edge of Chirmintarman glacier (Fig. 1).

The area of the debris flow cut on the moraine pedestal is 72 000 m^2. Morphometric properties of the debris flow site were estimated from Kanopus-V1 images acquired on October 6, 2015 and July 26, 2016. According to these data, the cut length at elevations 3800–4150 is 800 m, average width is 90 m, maximum width is 400 m [*Chernomorets et al., 2015; Dokukin et al., 2019*], and estimated depth reaches 50 m (Fig. 2).

The period of long-lasting positive temperatures resulting in the intense snow melting on the glacier and in the periglacial area is the main cause of catastrophic debris flow. Fluctuations of the temperatures within the debris flow site according to hourly ERA5 reanalysis at 30-km resolution performed by the European Centre for Medium-Range Weather Forecasts (ECMWF) are shown in Fig. 3.

The rise in temperature had been observed for two weeks before the catastrophe and reached the maximum (20°C) on July 16, 2015. In July 2014, the mean monthly temperature in this area was 9°C.

The length of the debris flow path from the source to the discharge point at the confluence of the Barsemdara and Gunt rivers was 7250 m with the average slope of 13.5°. According to M. Keiler's assessment [*Keiler et al., 2018*], the total volume of debris flow mass reached 4.2 M m^3. The debris flow mass dammed the Gunt River, so that Barsemkul' dammed lake with the area of 378 000 m^2 and max volume of about 4 M m^3 was formed [*Chernomorets et al., 2015*].

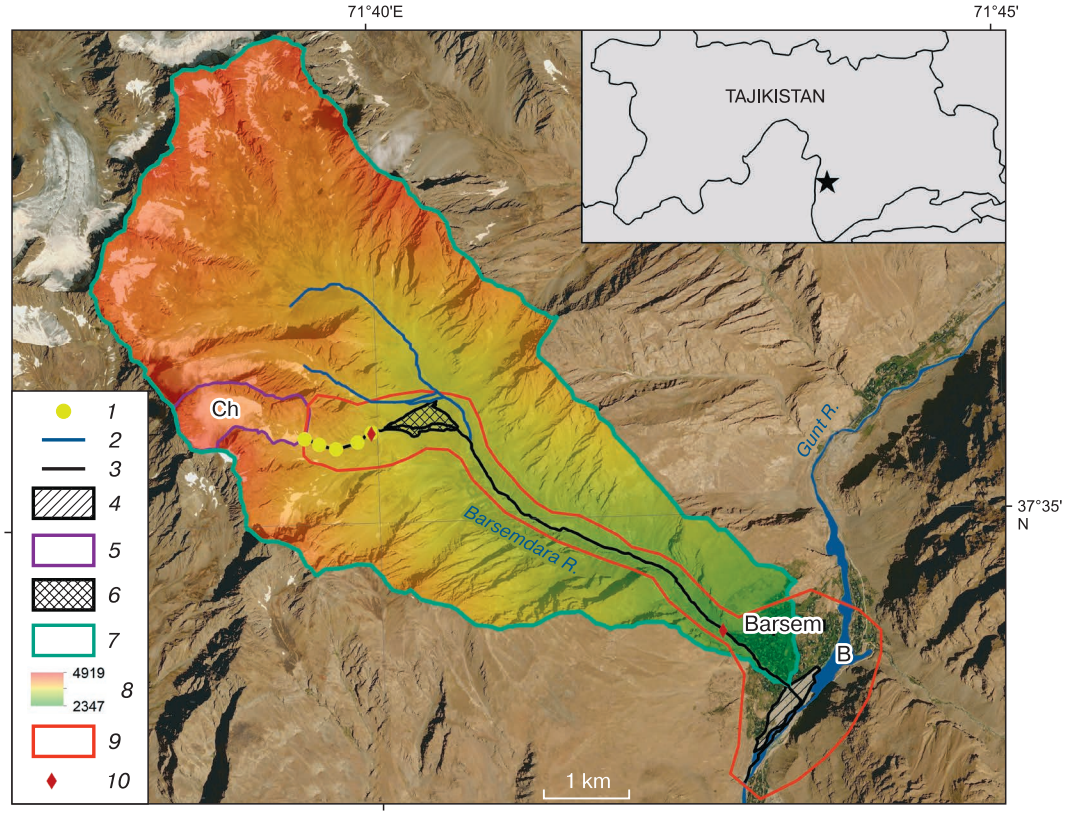

Fig. 1. The Barsemdara River catchment.

1 – areas within the debris flow site for the transport-shift model; *2* – streams, *3* – area of debris flow movement in 2015; *4* – section of intermediate debris flow accumulation in 2015; *5* – debris flow site boundaries; *6* – debris cone in 2015; *7* – Barsemdara River catchment; *8* – elevation, m; *9* – FLO-2D modelling extent; *10* – FLO-2D modelling sites; Ch – Chirmintarman Glacier; B – Barsemkul' Lake.

Fig. 2. Debris flow site in the Barsemdara River valley.

Photo by S.S. Chernomorets, 2019.

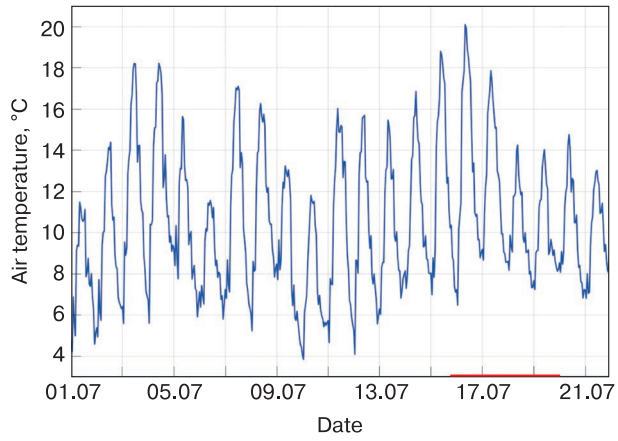

Fig. 3. Hourly air temperatures for the period from 1 to 21 of July, 2015 over the debris flow site according to ERA5 reanalysis data.

Red line is the debris flow activity.

Later, the area of this lake was reduced to 300 000 m^2 due to the construction of a discharge channel [*Dokukin et al., 2019*].

However, the danger of Lake Barsemkul' potential outburst flood is still preserved. Khorugh – the administrative center of the GBAO – is found just 15 km downstream the Gunt River. Earlier, a bathymetric survey of the lake was carried out [*Chernomorets et al., 2015*]. Moreover, possible scenarios of the lake outburst potentially resulting from (i) some lowering of the dam-break point, (ii) repeated debris flow from the Barsemdara valley, or (iii) outbursts in the cascade of glacial lakes triggering the catastrophic debris flow from the neighboring Sharipdara River valley were also discussed [*Kidyaeva et al., 2018*].

METHODS AND INPUT DATA

In this study, we applied a chain of numerical models, including the transport-shift model of debris flow formation, for calculating flow characteristics at the source site [*Vinogradov, 1980a,b*] and a hydrodynamic model FLO-2D for the valley zoning [*O'Brient et al., 1993*].

Transport-shift model of debris flow formation. The choice of the transport-shift model of debris flow formation was conditioned by the possibility to consider the increment of material in the forming debris flow. This is a one-dimensional model, and it is applied for calculating high-density debris flows. Model equations were developed by Yu.B. Vinogradov on the basis of debris flows experiments in the catchment of the Chemolgan River [*Vinogradova, Vinogradov, 2017*]. Earlier, modelling results were compared with observation data and were found to be satisfactory [*Vinogradova, Vinogradov, 2017*]. The model equations for calculating the discharge of solid material and the discharge and density of debris flow are now implemented into Python environment. The discharge of solid material is calculated first. Herewith, areas with approximately similar slopes and morphometric properties are delineated within the debris flow site. The main equation is solved not for the target variable G, but for the argument l [*Vinogradova, Vinogradov, 2017*]:

$$l = \left[\frac{Q\rho_0}{\varsigma\rho_0 + \rho} \ln \frac{Q\rho_0 + (\varsigma\rho_0 + \rho)G}{Q\rho_0 + (\varsigma\rho_0 + \rho)G_0} - \right.$$

$$\left. - \frac{Q}{\varsigma - \theta_{pp}} \ln \frac{Q + (\varsigma - \theta_{pp})G}{Q + (\varsigma - \theta_{pp})G_0} \right] \times$$

$$\times \left[A \frac{\mathrm{tg}\alpha}{\mathrm{tg}\varphi} g \sin\alpha \left[Q\rho_0 (\varsigma - \theta_{pp}) + Q(\varsigma\rho_0 + \rho) \right] \right]^{-1} + l_0, \quad (1)$$

where l is the distance along the thalweg of debris flow site, m; l_0 is the distance to the current sector, m; G is the solid material discharge, m^3/s; G_0 is the initial value of G for the certain sector and the previous upper sector (for the first upper sector $G_0 = 0$), m^3/s; α is the thalweg slope at the debris flow site, degrees; Q is the water discharge, m^3/s; φ is the static angle of internal friction of sediments, degrees; θ_{pp} is the ratio of the volume of water to the volume of solid material in the debris flow sediments at the liquid limit (in a stable immobile state); ζ is the ratio of the volume of water to the volume of solid material of debris flow sediments (dimensionless), g is the acceleration of gravity, m^2/s; ρ_0 is water density, kg/m^3; ρ is the density of debris flow sediments at the potential flow state, kg/m^3; and A is the coefficient of proportionality, m/(s^2·kg) [*Vinogradov, Vinogradova, 2010*]. According to scarce data of debris flow simulation under natural conditions, coefficient A was estimated to be in the range

of (3–5)·10^{-6} m/(s^2·kg), closer to 5·10^{-6} m/(s^2·kg) [*Vinogradova, Vinogradov, 2017*]. The debris flow discharge at the site of its origin (Q_{df}) can be calculated using Eq. (2):

$$Q_{df} = Q + (1 + \zeta)G, \quad (2)$$

where Q is the discharge of water entering the source of debris flow, m^3/s. The maximum debris flow discharge with the forward wave was estimated via multiplying its discharge at the outlet site by coefficient 2.5 (first approximation) [*Vinogradov, Vinogradova, 2010*].

The density of debris flow (y) moving along the site, is calculated by Eq. (3) [*Vinogradov, Vinogradova, 2010*]:

$$y = \frac{Qp_0 + (\varsigma p_0 + p)G}{Q + (1+\varsigma)G}. \quad (3)$$

Increment in the debris flow mass and changes in its density and discharge for each section along the site length are determined. As the input data in hydrodynamic models are hydrographs rather than a single discharge value, we have improved the transport-shift model via adding equations to calculate the wave velocity and lag time.

Most of the equations for calculating velocity of debris flows include such characteristics as the debris flow density, flow velocity, and empirical coefficients only. Herewith, empirical coefficients are obtained from observation data on particular debris flow catchments [*Golubtsov, 1969; RD 52.30.238-90, 1990*], or from laboratory experiments. Significant discrepancies have been found while comparing the observed velocities of debris flows at Chemolgan experiments and their calculated model values [*Sokolova et al., 2018*].

In this study, we have applied the equation for calculating debris flow velocity proposed by Yu.B. Vinogradov [*Vinogradov, Vinogradova, 2010*]. This equation includes not only the flow slope and depth but also internal angle of sediment friction, flow density, and various coefficients. To simplify the main equation, Vinogradov introduced three additional parameters:

$$M = \mu/(2\gamma\beta^2),$$

$$N = g\,(\sin\alpha - \mathrm{tg}\varphi^*\cdot\cos\alpha)/\beta^2,$$

$$S = gh\,\sin\alpha/\beta^2,$$

where μ is the coefficient of dynamic viscosity, Pa·s; γ is the debris flow density, kg/m^3; β is the mixing resistance coefficient, dimensionless; α is the slope of the debris flow thalweg, degrees; φ^* is the dynamic angle of internal friction of the sediments, degrees; g is the acceleration of gravity, m^2/s; and h is the flow depth, m. The final equation for calculating the maximum debris flow velocity (Vm) takes the form [*Vinogradov, Vinogradova, 2010*]:

$$Vm = \left(\frac{1}{1.5Nh}\right)\left[\left(\frac{M^2}{h^2} + S + Nh\right)^{1.5} - \left(\frac{M^2}{h^2} + S\right)^{1.5}\right] - \frac{M}{h}. \quad (4)$$

Herewith, the internal friction of debris flow sediments is expressed through μ, β, and φ^*. Viscosity factor (μ) characterizes the friction that occurs when individual layers and various elements slide over each other. With an increase in the size of the inclusions, their interaction also increases, i.e., more energy is dissipated, the viscosity factor varies between 100 and 1000 Pa·s. Mixing resistance coefficient (β) is the relative average distance perpendicular to the longitudinal axis of the debris flow, which the elements of the debris flow should pass before being involved in the general longitudinal motion. Its values vary between 0.1 and 0.5 [*Vinogradov, Vinogradova, 2010*].

Initial flow depth value for calculating the debris flow velocity was considered equal to 1 m at each section. Knowing the debris flow discharge and velocity, one can obtain its approximate cross-sectional area. The flow width was estimated using various satellite data at 15 to 30 m spatial resolution. Then, the flow depth was recalculated, and the resulting values were substituted into Eq. (4). To estimate the wave propagation time, the distance between the boundaries of the sections was divided by the velocity value.

Topographic data were extracted from digital elevation model ALOS PALSAR acquired on August 8, 2007 (12.5 m spatial resolution) [*https://search.asf.alaska.edu/#/*]. In total, four sectors with approximately similar morphometric characteristics were delineated within the debris flow channel (Fig. 1).

The input hydrograph for calculations was created for the first three debris flow waves based on the information obtained from local residents. The first wave was registered on July 16 at 14:30. According to eyewitnesses, the most powerful third wave took place on the same day less than an hour after the first and second waves. According to field survey in August 2019 carried out jointly by specialists from the Faculty of Geography of Moscow State University and the Aga Khan Agency for Habitat (AKAH), the discharge in front of the debris flow site during the third wave was estimated at 25 m^3/s. The base discharge in the upper reaches was estimated at 5 m^3/s. In the following days, floods and small debris flows were observed along the valley that were formed due to the natural snow melting and had no destructive power [*Chernomorets et al., 2015*]. Figure 4 shows the input hydrograph; the starting point corresponds to 14:30 (July 16, 2015).

Density of debris flow-forming deposits ρ was taken equal to 2600 kg/m^3; water density ρ_0, 1000 kg/m^3. The mean thalweg slope was 13.5°. The angles of internal friction of the sediments – static φ and dynamic φ^* – were estimated at 40° and 22°, respectively, according to construction design rules [*SP 425.1325800, 2019*], survey reports of the North Caucasian Institute for Water Management and Land Reclamation (Sevkavgiprovodkhoz) [*Nikulin, 2009*], and works of Yu.B. Vinogradov [*Vinogradov, Vinogra-*

dova, 2010]. Earlier, we presented the calculations of this debris flow for three scenarios of the initial water content of the deposits: completely dry, moistened to the liquid limit, and inundated [*Kurovskaia et al., 2020*]. We also compared model characteristics with the values of the debris flow velocity and discharge at the outlet as estimated from video records. It was found that the best fit of the model to the factual observations was in the case of rock moistening to the liquid limit. In this paper, we consider only this option for further calculations.

Hydrodynamic model FLO-2D. A two-dimensional hydrodynamic model FLO-2D [*O'Brien et al., 1993*] was used to estimate the distribution of flow velocities and depths within the channel. This model is widely applied in scientific research related to the dynamics of water and debris flows [*Cesca, D'Agostino, 2008; Mikhailov, Chernomorets, 2011; Petrakov et al., 2012; Wu et al., 2013*]. It is based on the solution of Saint-Venant equations, in which the flow characteristics are averaged over depths (the so-called shallow-water equations) [*Cunge et al., 1980*]. When modeling debris flow in the FLO-2D model, it is assumed that it moves as a Bingham fluid (viscous-plastic fluid) [*O'Brien et al., 1993*]. The model operates with the following input data: topographic maps and topographic survey data synthesized in digital elevation models (DEM), background discharges and levels of the water in the main channel and tributaries, and input hydrograph and its shape. As an output, the model gives depths, velocities, and levels of water or debris flow surfaces, as well as other flow parameters in plane.

As the input hydrological information, we used hydrographs obtained from the transport-shift model. For scenario I, we used discharges of the forward wave as an input hydrograph; for scenario II, debris flow discharges at the site outlet. Background discharge of the Gunt River was taken at 100 m^3/s. This value corresponds to the average discharge over the observation period and the discharge of 50% probability.

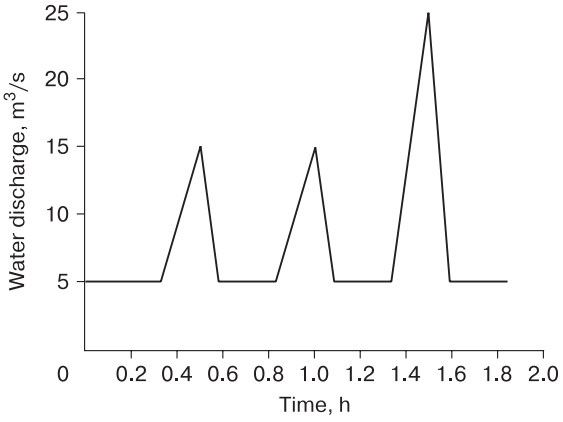

Fig. 4. Input hydrograph for debris flow modeling.

We used digital elevation model from ALOS PALSAR (12.5 m resolution) acquired on August 8, 2007 as input topographic data [*https://search.asf.alaska.edu/#/*]. After correction, the DEM was re-interpolated with the cell size of 12.5 m to be used in the FLO-2D model. Further, we used unmanned aerial vehicle (UAV) data for the area of the debris cone obtained during the field survey by the authors in August 2019. UAV-based DEM was resampled to 5 × 5 m grid. We also used bathymetric data for Lake Barsemkul' surveyed in 2017.

The input parameters for the FLO-2D model were also volumetric concentration of sediments in the debris flow, plastic friction stress, and flow viscosities. Concentration of sediments was set to be 45%, which corresponds to incoherent debris flow with intensive mixing [*O'Brien et al., 1993*]. If it is impossible to conduct a detailed rheological analysis of debris flows, the following empirical formulas are used to calculate the plastic friction stress and flow viscosity in the model:

$$\eta = \alpha_1 \exp(\beta_1 C_v); \quad (5)$$

$$\tau_y = \alpha_2 \exp(\beta_2 C_v), \quad (6)$$

where τ_y is plastic friction stress, η is flow viscosity, and C_v is sediment volumetric concentration; $\alpha_{1,2}$, and $\beta_{1,2}$ are empirical coefficients determined in laboratory [*O'Brien, Julien, 1988*]. As seen from Eqs. (5) and (6), η and τ_y are functions of the volumetric concentration of sediments considering only the volume of silt, clay, and, in some cases, sand fractions. However, these equations do not consider coarse-grained sediments. The viscosity of a fluid is also a function of the volumetric concentration of sediments. The authors of the model estimated the parameters of these equations using debris flow samples collected in the Rocky Mountains, Colorado, near the cities of Aspen and Glenwood Springs. The values of the empirical coefficients α_i and β_i were obtained using regression analysis for each sample and are presented in Table 1 [*O'Brien, Julien, 1988*]. By default, parameter e is recommended for simulating the movement of a more viscous flow, and parameter a is recommended for less coherent flows, including sediment-water floods [*O'Brien, Julien,*

Table 1. **Parameters for calculating plastic flow stress and viscosity as a function of sediment concentration [*O'Brien, Julien, 1988*]**

Parameter set	Debris flow deposit sample	Parameters for calculating plastic friction stress		Parameters for calculating flow viscosity	
		α_2	β_2	α_1	β_1
a	Aspen natural soil	0.1520	18.7	0.001 36	28.4
b	Glenwood 1	0.0345	20.1	0.002 83	23.0
c	Glenwood 2	0.0765	16.9	0.064 80	6.2
d	Glenwood 3	0.000 707	29.8	0.006 32	19.9
e	Glenwood 4	0.001 72	29.5	0.000 602	33.1

1988]. Since there were no field data for the studied catchment, simulation was performed using several sets of parameters presented in Table 1.

MODELING RESULTS

We have obtained flow discharge values for each of the four sectors within the debris flow site by applying Eqs. (1) and (2). Flow velocities are required for debris flow hydrographs. The results of velocity calculations according to Eq. (4) for each sector and for the forefront wave are presented in Table 2.

Calculations for the first two waves and for the third wave were separately performed, because water discharge values for first two waves entering the channel were the same and equal to 15 m^3/s. Flow density values calculated using Eq. (3) were then used in calculations of the velocity. As seen from Table 2, flow velocities differed among sectors. Average velocity for the first two waves (excluding the forefront wave) was 13.4 m/s; the third wave had the flow velocity of 13.2 m/s.

Figure 5 shows hydrographs of debris flow waves for all four sectors within the site and the maximum discharge values for the forefront wave. A gradual increase in the flow discharge from the first to the fourth sector is clearly seen.

For the first two waves, debris flow discharge along the entire site increased from 145 to 391 m^3/s. According to approximate estimates, the discharge of the forefront wave reached 978 m^3/s. For the third wave, the discharge increased from 255 to 625 m^3/s from the first to the fourth sector; the discharge of the forefront wave reached 1630 m^3/s. Minimum debris flow discharge time (13 s) was found for the first and fourth sectors. and maximum discharge time (22 s) was found for the third sector. Time lag of the front wave in the fourth sector varied from 18 to 20 s.

Further, we performed a zoning of the valley using FLO-2D model. As noted earlier, two simulation scenarios were considered. In scenario I (for the forefront wave), the discharge changed significantly depending on the input values of plastic friction stress and flow viscosity (Table 3).

The most realistic results, close to the estimates based on field data, were obtained using option Ib. Calculations with other options are given for comparison to show how the use of different debris flow parameters in the FLO-2D model affects the results. Thus, the flow rates for option Ib were from 1494 to 2860 m^3/s for individual waves, while the flow rate estimated from video records was 1536 m^3/s, and the velocity was 16.6 m/s [*Kurovskaia et al., 2020*]. Note that we used records for one of 40 debris flow waves,

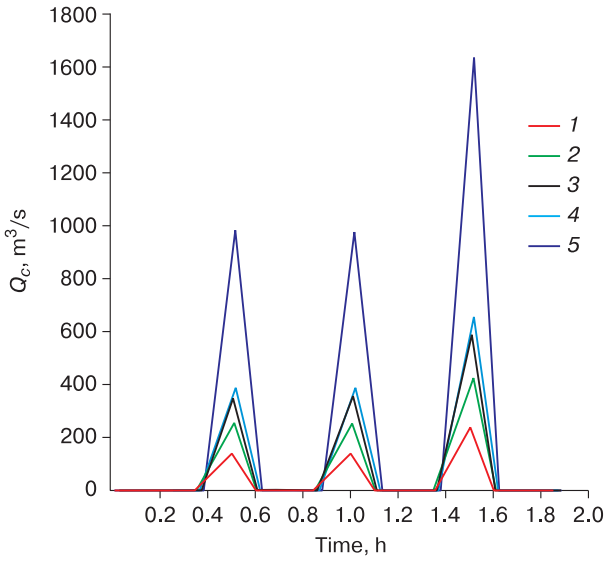

Fig. 5. Debris flow hydrographs for the four sectors of the debris flow site (lines *1–4*) and for the forefront wave (line *5*) obtained as transport-shift model output.

Table 2. **Debris flow velocity**

Sector number	Slope, degrees	Flow depth for the first and second waves, m	Velocity of the first and second waves, m/s	Flow depth for the third wave, m	Velocity of the third wave, m/s
1	28.2	2.2	14.6	2.0	15.0
2	26.6	2.0	13.9	2.1	14.3
3	24.6	2.1	13.1	2.3	13.1
4	20.4	2.8	11.2	2.3	11.2
5 (forefront wave)	20.4	4.0	8.3	6.2	7.2
Entire site	25.2	2.7	12.4	3.0	11.9

Table 3. **Results of hydrodynamic modelling for scenarios I and II**

Calculation option	Max discharge, m^3/s (first wave)	Passing time, min	Max discharge, m^3/s (second wave)	Passing time, min	Max discharge, m^3/s (third wave)	Passing time, min
Ia	855	15.6	1477	5.4	2513	12.0
Ib	1494	12.6	1639	12.0	2860	9.6
Ic	1433	9.0	1378	7.8	3297	3.0
Id	977	11.4	1744	12.0	2993	9.0
Ie	430	21.0	1134	4.8	1939	3.0
IIa	164	18.2	674	9.1	1322	6.7
IIb	295	21.1	554	9.1	648	15.1
IIc	777	9.7	1153	11.5	1045	8.5
IId	412	18.7	404	13.9	683	15.1
IIe	30	21.1	394	10.9	580	8.5

presumably the third, the most destructive, so we obtained approximate estimates.

The highest discharge of the forefront wave at the top of debris cone was 3297 m^3/s during the third wave according to Ic option. Debris flow discharges for the first and second waves were lower than the values assessed using video records. Minimum values for the top of debris cone were obtained for option Ie (most viscous flow). The discharge for the first and second waves was 430 and 1134 m^3/s, respectively. The discharge for the third wave was by 403 m^3/s higher than the value estimated using video records. Herewith, parameters of option e are recommended for cement-like debris flow, which was not the case for the observed debris flow. Slightly higher discharges were obtained for the parameters of option Ia typical for a low-density debris flow. The discharge of the first wavy reached 855 m^3/s; the discharge of the second wave was 60 m^3/s lower than the video-based estimate. For the third wave, the simulated discharge was 1.6 times higher than the video-based estimate. In option Id, the discharge of the first wave reached 977 m^3/s; the discharges of the second and third waves exceeded the video-based estimates by 1.1–1.9 times.

Then, the same parameters were used to simulate debris flow discharges at the site outlet according to scenario II.

The highest discharge of the third wave at the top of debris cone was 1321 m^3/s according to option IIa. For the first and second waves, discharge values were 164 and 674 m^3/s, respectively. The highest discharges for these two waves were obtained using option IIc: 777 and 1153 m^3/s, respectively. The minimum debris flow discharge of the first wave (30 m^3/s) was obtained using option IIe. For the second and third waves, the discharge varied from 394 to 560 m^3/s. In general, options IIb and IId were close to one another; discharge values changed from 295 to 683 m^3/s.

For calculating the debris flow characteristics at the debris cone, we used the set of parameters b as the most realistic one. The discharge in this case was close to the value obtained from video records [*Kurovskaia et al., 2020*]. To estimate the maximum possible discharge at the debris cone, we made a calculation using a set of parameters c.

Discharges at the debris cone calculated using option Ib (scenario I) varied between 556 and 2181 m^3/s. The flow passed this section of debris cone in 1.8–4.8 min. The flow velocity in the Barsemdara River channel exceeded 5 m/s; in the adjacent area, is was up to 3.2 m/s (Fig. 6*b*). A considerable number of buildings on the left bank of the river were within the flood zone. The distribution of depths in the flow is shown in Fig. 6*a*.

According to scenario II, discharges within the debris cone changed from 101 to 543 m^3/s. The spreading of the first wave was wherein observed. The flow travel time was from 6 to 7.8 min. The flow depth within the debris cone averaged 4.8 m reaching 9.5 m in some areas. The debris flow velocity in the Barsemdara and Gunt rivers, as well as within the debris cone, was 5 m/s.

When modeling the passage of the forefront wave, the debris flow discharge at the debris cone turned out to be much higher and ranged from 1580 to 3351 m^3/s for the third wave according to option c. Lag time varied from 0.6 to 1.2 min. Maximum debris flow velocities within the Barsemdara River channel and in the adjacent area were 19.4 and 10.8 m/s, respectively. Flow depth within the debris cone varied

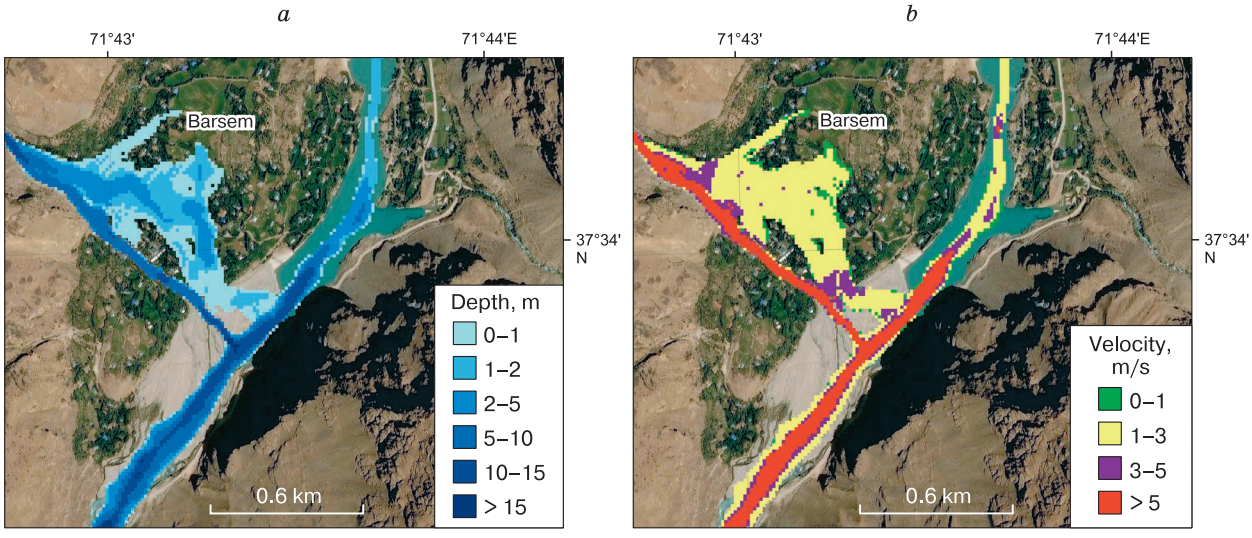

Fig. 6. Plane distribution of flow parameters for the 2015 debris flow simulated using FLO-2D model according to scenario I, parameter set b.

a – flow depth, *b* – flow velocity.

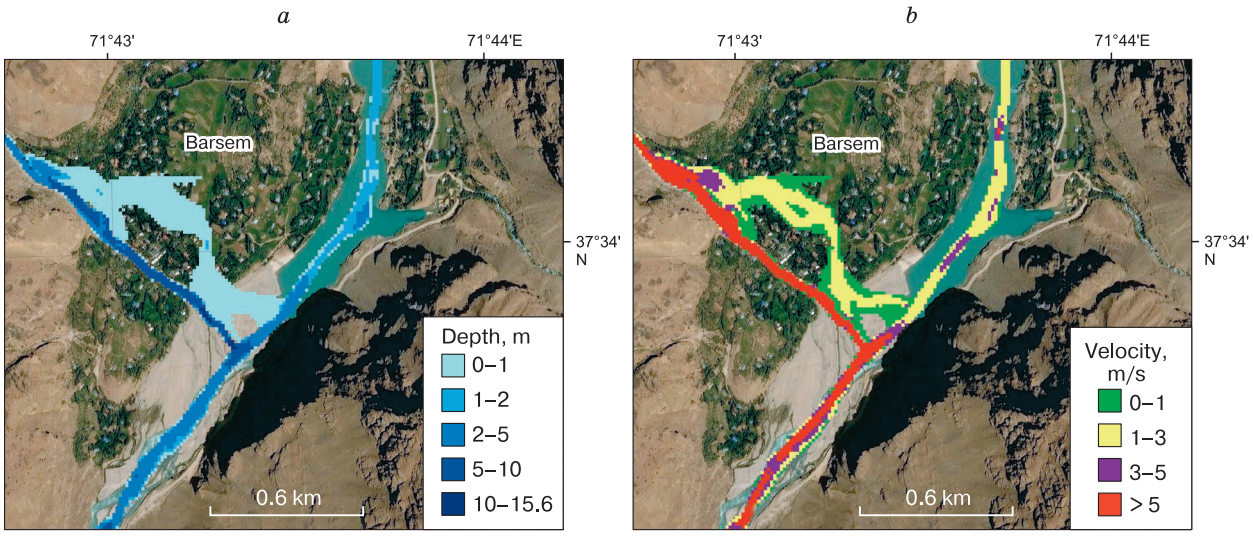

Fig. 7. Plane distribution of flow parameters for the 2015 debris flow simulated using FLO-2D model according to II scenario, parameter set c.

a – flow depth, *b* – flow velocity.

from 1 to 5 m and was up to 15 m in the Barsemdara River channel.

The debris flow discharges for option c (scenario II) were 534–840 m^3/s. The lag time of the waves varied from 0.6 to 1.8 min. At the debris cone section, the maximum debris flow velocity within the Barsemdara River channel was 15.1 m/s; on the adjacent area, it reached 6.7 m/s; in the Gunt River channel, 11.8 m/s (Fig. 7).

A comparison of modeling and observation data indicates that, in reality, there was no flow spreading along the debris cone to its left side. Waves passed exclusively within the Barsemdara River channel, despite its lowered left bank (Fig. 8). Thus, the flow incised into the surface of the debris cone.

Fig. 8. Barsemdara River channel.

Photo by S.S. Chernomorets, 2019.

One of the reasons for the inconsistency of factual and simulated flood zones within the cone could be due to erosional processes that are not considered in the FLO-2D model calculation, except for the initial input morphometric data. In our study, we used satellite images of 12.5-m resolution, which smoothed meso- and microtopographic features. However, this was the only option available for this valley before the debris flow of 2015.

Calculations of potential modern debris flow in the Barsemdara valley were made using 2019 UAV-based DEM covering the debris cone, hydrographs (scenario I) in the FLO-2D model with parameter sets b (as the most realistic one) and c (giving maximum values). These calculations reflect the flood-prone zones in case of the repeated debris flow and the modern topographic conditions.

Modelling using the set of parameters b indicates that the flow is almost entirely concentrated within the Barsemdara channel above the debris cone, while the cone is flooded (Fig. 9). During the debris flow in 2015, the debris cone was not flooded. According to 2019 UAV-based DEM data, the debris cone is characterized by a sharp change in the heights (from 2541 to 2519 m asl). This can cause the flooding of the territory in case of another intense debris flow.

The results obtained with parameter set c indicate that in the event of a similarly strong debris flow, not only the debris cone but also houses near the Barsemdara River channel upstream the cone will be in the flood-prone zone. Flow depth for both sets of parameters will vary from 8 m on the debris cone to 15 m in the Barsemdara River channel.

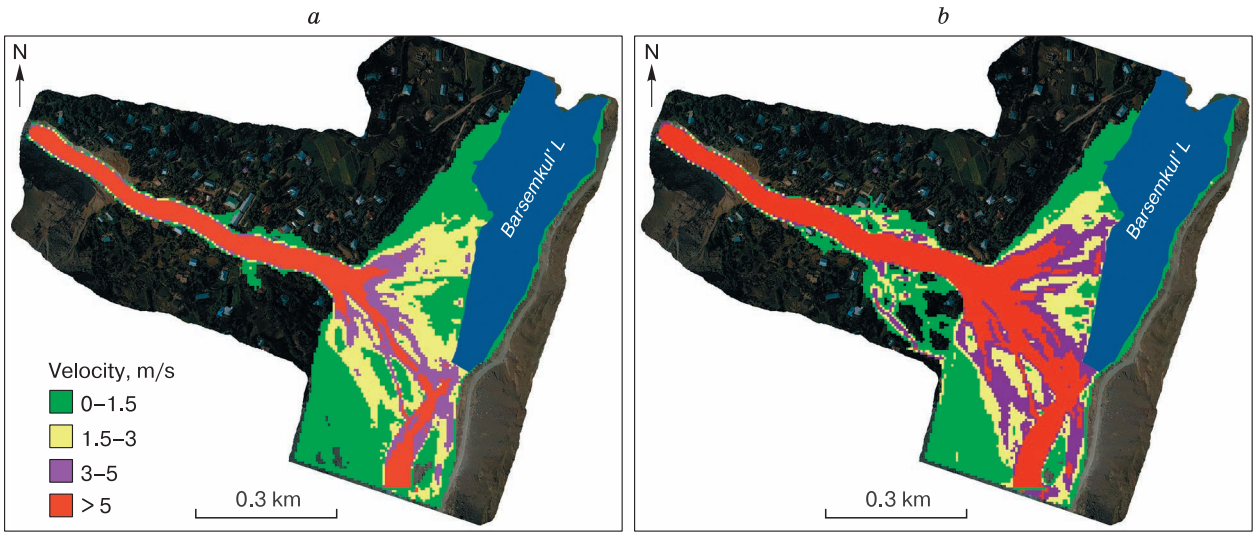

Fig. 9. Plane distribution of the flow velocity of the first wave simulated using FLO-2D model and UAV data according to scenario I.

a – scenario Ib, *b* – scenario Ic.

The Barsemdara channel topography was relatively stable before 2015. After the catastrophe, the topography has stabilized and there are no changes now. In case of using high-resolution DEM data, we should bear in mind that debris cones are unstable landforms, and their topography is subjected to changes after each high-water event. Intense water flood or debris flows can form a new channel in the area of the village beyond the current channel. The FLO-2D model does not consider erosional processes. Therefore, in case of catastrophic high-water event, the flood zone picture may change significantly. At the same time, initially such a territory may not be identified as potentially dangerous when modeling with the use of available UAV-based DEM data. In fact, such high-resolution DEMs rapidly become outdated. More accurate results for the moment will be obtained using detailed modeling on the basis of state-of-the-art DEM. Therefore, it is better to assess flood-prone zones regularly. The application of a publicly available 12.5-m resolution DEM is suitable for obtaining a quick generalized assessment of potentially hazardous areas, as well as for calculating past debris flows.

CONCLUSIONS

In this work, we have assessed the possibility to apply chain modeling for calculating the debris flow in the Barsemdara River valley in 2015, including models for calculating the debris flow characteristics at the site and while moving along the valley. We have used transport-shift model to calculate the debris flow characteristics at the site. A distinctive feature of this model is the ability to estimate the increment of solid material during the formation of a debris flow and the relative simplicity of the input information, which is especially important in conditions of insufficient data.

We improved the model via adding the calculation of the flow velocity according to the equation suggested by Yu.B. Vinogradov and of the time of the wave passing. These improvements made it possible to obtain physically substantiated discharge hydrographs for the first three most destructive flow waves. We further conducted the valley zoning using the hydrodynamic model FLO-2D. Transport-shift model outputs – discharges of forefront wave (scenario I) and at the site outlet (scenario) – were used as input hydrographs. As it was impossible to conduct laboratory experiments to refine the parameters in the formulas for calculating the plastic friction stress and flow viscosity, we carried out experimental calculations with five options of parameter sets. Thus, the discharge values with set b (Table 3) at top of the debris cone varied from 1494 to 2860 m^3/s for the first and third waves (scenario I). The highest forefront wave discharge (3297 m^3/s) was obtained with parameter set c for the third wave. Discharges for the first and second waves were slightly lower (1433 and 1378 m^3/s). Discharges obtained using parameter set b (scenario I) varied between 556 and 2181 m^3/s in the section of debris cone. Though the discharge values calculated with this set of parameters are overestimated as compared with video-based estimates, the authors believe that parameter set b is more probable for a particular debris flow.

Given the resolution of the satellite-based DEM (12.5 m) used in the calculations, the flood zone turned out to be much larger than the actual data observed in 2015. This discrepancy of field and modeling data is explained by the generalization of local topographic features on satellite data of such a resolution. We have therefore performed an additional modeling with the use of UAV data collected in 2019 as input data. The results of calculations illustrate the flood zone during the passage of a debris flow of similar intensity over the modern topography. For the parameter set b, the debris flow is completely concentrated in the channel down to the top of the debris cone with subsequent spreading. Modeling with the parameter set c indicates that not only the debris cone but also houses near the Barsemdara River channel will be in the flood zone. In general, our results attest to the applicability of the considered chain of mathematical models for the assessments of flood zones.

Acknowledgements. *The authors express their gratitude to F.O. Marodaseynov and A. Akdodov from the Aga Khan Agency for Habitat and I.V. Krylenko and K.S. Viskhadzhieva from Moscow State University for their help in field data collection.*

Funding. *This study has been carried out within the framework of state assignments of the Lomonosov Moscow State University, sections I.7 (CITIS 121051300175-4) and I.10 (CITIS 121051400038-1) and the Water Problems Institute of the Russian Academy of Science, theme 0147-2019-0001 (CITIS AAAA-A18-118022090056-0) and supported by the Russian Foundation for Basic Research (project no. 20-35-90006).*

References

Cesca M., D'Agostino V., 2008. Comparison between FLO-2D and RAMMS in debris-flow modelling: a case study in the Dolomites. *WIT Transactions on Eng. Sciences*, vol. LX, 197–206.

Chernomorets S.S., Savernyuk E.A., Bobov R. et al., 2015. Mudflows in the valley of the Barsemdara River in July 2015 and the dammed lake Barsemkul on the Gunt River (Gorno-Badakhshan Autonomous Region, Tajikistan). In: Proc. Int. Conf. Second Vinogradov's Readings. The Art of Hydrology (St. Petersburg, Nov. 18–22, 2015). St. Petersburg, Saint-Petersburg State University, p. 261–264 (in Russian).

Cunge J.A., Holly F.M., Verwey A., 1980. Practical Aspects of Computational River Hydraulics. London, Pitman. Translated under the title Chislennye Metody v zdachakh Rechnoi Gidravliki (Moscow, Energoatomizdat, 1985), 255 p. (in Russian).

Dokukin M.D., Chernomorets S.S., Savernyuk E.A. et al., 2019. Barsem debris flow disaster in the Pamirs in 2015 and its analogues in the Central Caucasus. *Georisk,* **XIII** (1), 26–36 (in Russian).

Golubtsov V.V., 1969. On hydraulic resistance and the formula for calculating the average flow rate of mountain rivers. *Proc. KazNIGMI,* 33, 30–41 (in Russian).

Keiler M., Zimmermann M., Bigler S., Fuchs S., 2018. Assessing a large-scale debris flow in Barsem, Tajikistan: exceptional size, duration and process chain. In: Proc. European Geosciences Union General Assembly Conf. (Vienna, April 8–13, 2018), Vienna, Austria, p. 5405.

Kidyaeva V.M., Chernomorets S.S., Savernyuk E.A. et al., 2018. Modeling of breakthroughs of mountain lakes and mudflows in the Gorno-Badakhshan Autonomous region, Tajikistan. In: Proc. III Int. Conf. Facets of Hydrology (St. Petersburg, March 28–30, 2018). St. Petersburg, St. Petersburg State Univ., p. 897–902 (in Russian).

Kotlyakov V.M. (Ed.), 1984. Glaciological Dictionary. Leningrad, Gidrometeoizdat, 528 p. (in Russian).

Kurovskaia V.A., Chernomorets S.S., Vinogradova T.A. et al., 2020. Assessment of the quantitative characteristics of the mudflow in the Barsemdara River valley (Tajikistan) in 2015 based on video materials and modeling results. *Georisk*, **XIV** (3), 12–22 (in Russian).

Mal'neva I.V., Kononova N.K., 2012. Mudflow activity in Russia and neighboring countries in the XXI century. *Georisk,* **IV** (4), 48–54 (in Russian).

Mergili M., Schneider D., Worni R., Schneider J., 2011. Glacial lake outburst floods in the Pamir of Tajikistan: Challenges in prediction and modelling. In: Proc. Fifth Int. Conf. Debris-Flow Hazards Mitigation: Mechanics, Prediction, and Assessment (Padua, June 14–17, 2011). Padua, Italy, p. 973–982.

Mikhailov V.O., Chernomorets S.S., 2011. Mathematical Modeling of Mudflows, Collapses and Landslides. Moscow, Lambert, 131 p. (in Russian).

Musoev Z., Atlas L.I. (Eds.), 1980. Basins of the right tributaries of the Panj River from the mouth of the Vakhsh River to the mouth of the Vanj River (chapter 10), The Vostochnyi Kyzylsu River basin (chapter 19). In: Catalogue of Glaciers of the USSR. Vol. 14. Central Asia. Issue 3. Amu Darya. Leningrad, GIMIZ, 56 p. (in Russian).

Nikulin A.S., 2009. Experience in determining the angles of internal friction of mudflow undercoats. In: Collection of Scientific Works of JSC Sevkavgiprovodkhoz, iss. 18, 30–33 (in Russian).

O'Brien J.S., Julien P.Y., 1988. Laboratory analysis of mudflow properties. *J. Hydraul. Engin.,* CXIV (8), 877–887.

O'Brien J.S., Julien P.Y., Fullerton W.T., 1993. Two-dimensional water flood and mudflow simulation. *J. Hydraul. Engin.,* CXIX (2), 244–261.

Osipova G.B. (Ed.), 1978. The Vanj River basin (chapter 11), The Yazgulem River basin (chapter 12). In: Catalogue of Glaciers of the USSR. Vol. 14. Central Asia. Issue 3. Amu Darya. Leningrad, GIMIZ, 84 p. (in Russian).

Petrakov D.A., Tutubalina O.V., Aleinikov A.A. et al., 2012. Monitoring of Bashkara Glacier lakes (Central Caucasus, Russia) and modelling of their potential outburst. *Nat. Hazards,* LXI (3), 1293–1316.

RD 52.30.238-90, 1990. Management of Mudflow Stations and Hydrographic Parties. Vol. I. Moscow, Gidrometeoizdat, 199 p. (in Russian).

Shchetinnikov A.S. (Ed.), 1979. The Marghab River basin (chapter 14). In: Catalogue of Glaciers of the USSR. Vol. 14. Central Asia. Issue 3. Amu Darya. Leningrad, GIMIZ, 91 p. (in Russian).

Shchetinnikov A.S., Podkopaeva L.D. (Eds.), 1978. The Bartang River basin (chapter 13). In: Catalogue of Glaciers of the USSR. Vol. 14. Central Asia. Issue 3. Amu Darya. Leningrad, GIMIZ, 107 p. (in Russian).

Sokolova D.P., Vinogradova T.A., Ostashov A.A., 2018. Comparison of various methods for calculating the rate of mudflow. *Georisk,* **VIII** (4), 76–86 (in Russian).

SP 425.1325800, 2019. Engineering Protection of Territories from Erosion. Design Rules. Moscow, Standartinform, 36 p. (in Russian).

Tukeev O.V., 2002. Mudflows in the Pamirs: Disasters, Patterns, Forecast. Moscow, VNII GOChS, 176 p. (in Russian).

URL: https://search.asf.alaska.edu/#/ (last visited: 28.10.2020).

Varnakova G.M., Rototaeva O.V. (Eds.), 1978. The Obikhingou River Basin (chapter 9). In: Catalogue of Glaciers of the USSR. Vol. 14. Central Asia. Issue 3. Amu Darya. Leningrad, GIMIZ, 110 p. (in Russian).

Varnakova G.M., Rototaeva O.V. (Eds.), 1979. The Gunt River basin (chapter 15). In: Catalogue of Glaciers of the USSR. Vol. 14. Central Asia. Issue 3. Amu Darya. Leningrad, GIMIZ, 126 p. (in Russian).

Vinogradov Yu.B., 1980a. Transport and transport-shift mudflow processes. In: Debris Flows. Almaty, KazNIGMI, iss. 4, 3–18 (in Russian).

Vinogradov Yu.B., 1980b. Etudes on Debris Flows. Leningrad, Gidrometeoizdat, 160 p. (in Russian).

Vinogradov Yu.B., Vinogradova T.A., 2010. Mathematical Modeling in Hydrology. Moscow, Academy, 304 p. (in Russian).

Vinogradova T.A., Vinogradov A.Y., 2017. The experimental debris flows in the Chemolgan River basin. *Nat. Hazards,* LXXXVIII, 189–198.

Wu Y.H., Liu K.F., Chen Y.C., 2013. Comparison between FLO-2D and Debris-2D on the application of assessment of granular debris flow hazards with case study. *J. Mountain Sci.,* **X** (2), 293–304.

Received July 15, 2021
Revised January 28, 2022
Accepted April 3, 2022

Translated by Yu.A. Dvornikov